NANOPARTICLE EFFECTS ON CELL MIGRATION

BY

YISHU ZHANG

THESIS

Submitted in partial fulfillment of the requirements
for the degree of Master of Science in Chemistry
in the Graduate College of the
University of Illinois at Urbana-Champaign, 2020

Urbana, Illinois

Adviser:

Professor Catherine J. Murphy

ABSTRACT

It has been found that gold nanoparticles (Au NPs) are excellent materials for biological applications such as diagnosis and drug delivery, which makes it crucial to understand the interface between gold nanoparticles and cells. Previous work has shown that gold nanoparticles can affect cellular migration, even if outside cells. However, the fundamental of interaction between Au NPs and cells has remained unclear. The most accepted mechanism currently is that by sequestering biomolecules from the environment nanoparticles can change the local molecular concentration, and thus influence cell behavior.

Chemotaxis is the movement of cells in response to a chemical stimulus. Chemoattractants are inorganic and organic substances, usually proteins, that create a concentration gradient that attracts cells to move towards them. Chemoattractants are known to be involved in immune responses and wound healing processes in eukaryotic cells. With the presence of chemoattractants, cells move directionally towards the infected sites or wound. Similar processes exist in wound healing.

To study the intervention of gold nanoparticles in chemotaxis, two systems were chosen. The first system that was examined in the human monocytes THP-1 cells. As a type of monocyte, THP-1 is known to migrate in response peptide formyl peptides. Another cell/chemoattractant pair that was examined was human dermal fibroblasts (HDF) and platelet-derived growth factor (PDGF). Cells were cultured and placed into 3D collagen gel in a specialized chemotaxis slide, in which a steady chemoattractant concentration was produced. Cell migration was recorded through bright-field optical microscopy. Gold nanospheres with different surface chemistries were

introduced into the system. Surface chemistries include cationic PDADMAC, and anionic PSS and citrate.

The hypothesis under consideration was that chemoattractant would adsorb mostly strongly to the nanoparticle of the opposite charge, thus affecting chemotaxis. A set of experiments was designed to test this hypothesis.

ACKNOWLEDGMENTS

I would like to thank my research advisor, Professor Catherine J. Murphy, for her support and guidance for me in the past three years at the University of Illinois at Urbana Champaign (UIUC). I've always been admiring how passionate and dedicated she is to science and I was strongly motivated and inspired by her. I also thank her for allowing me to explore science freely while guiding me in the right direction. Cathy is more than just a wise mentor to me. She is a great listener and tried her best to help me even though many times my problems were not related to the lab. I feel supported and encouraged when she is around.

I would also like to thank Professor Greg Girolami and Professor Josh Vura-Weis. I enjoyed the year-long advanced inorganic class very much. Their classes taught me not only chemistry knowledge but also how to be a good scientist. Professor Sandy McMaster has been extremely helpful in preparing cell media and giving me advice about my experiments and cell culture in general. My lab mates have been a great support to me as well. I want to thank Dr. Huei-huei Chang and Dr. Meng Wu both as colleagues and friends. They reached out to me when I had my surgery. They listened to my thoughts when I was lost and gave me advice.

I thank my family for their love and patience. I've always considered myself a problematic kid yet your love and attention have been a great source of motivation to me. I always feel lucky that I could be your kid. You've been great parents and friends to me. I can't put all my emotions into words, so I guess I will just say you will always be the people that I love the most in this world.

My friends have been my armor all this time as well. Great thanks to Miss. Jiachen Wang, who always make time to listen to me, talk to me and even travel all the way to see me when she is busy. She was there for me at my hardest moment and put up with my bad temper. It is the 10th

year that I know her and she is always there when I need here. I thank Miss. Chengyin Liu to cheer me up remotely. I think our friendship might be one of the best gifts I got this year and I wish to see you soon. I also want to thank Mr. Minghe Lou, who has been my best friend since high school and never stop supporting me no matter where he is. Last but not least, I want to thank my boyfriend Mr. Angel Nieves for always never leaving me alone. You've been such a nice and cheerful person to me and I see myself becoming a better person with you. I can't make this far without any of my friends.

I appreciate all the kindness that I got in the past three years. It was an experience that changed my life a lot at UIUC. I gain lots of experience in solving problems myself and learned to focus on this beautiful world more. I wish you all the best.

倾听我的独白

忍让我的固执

宽容我的借口

相信我的喋喋不休。

TABLE OF CONTENTS

CHAPTER 1: Introduction to Gold Nanoparticles and Their Biological Applications

1.1 Brief history of gold nanoparticles

Gold has been highly recognized and valued since pre-historic period[1]. It might even be the very first metal that was used for decorations and rituals[2]. Even though gold is not used as currency anymore, it is still considered as a symbol of wealth and achievement: gold is made into gold medals and awarded as the top prize to the winner. The applications of gold have been broadening due to their physical characters. Gold has the highest malleable of all metal. One gram of gold can be made into a one square meter thin film or 4000 meters thread[3]. Gold is also used heavily for electronics. Gold has a low electrical resistance, which has been used as part of electric wires. There are also records of people using gold as part of the cuisine or medicine.

Other than the bulk gold, gold on the nano-scale has been getting a great amount of attention due to its fascinating optical properties. One of the most well-known examples of utilizing colloidal gold is the Lycurgus cup, which changes color when the location of the light source changes. If the light comes from the interior of the cup it shows a ruby red color while if the light is reflected from the outside of the cup, it shows a jade green color[4]. The fascinating interactions between gold nanoparticles (generally between 1 nm and 100 nm) are not limited to unique colors. When exposed to light, a collective coherent oscillation of free electrons from the conduction band is induced. With the electron oscillation, charges separate and form a dipole along the direction of the electric field of the light[5]. This phenomenon of intense absorption and scattering of light is called localized surface plasmon resonance (LSPR). The resonance condition can be monitored by absorption or scattering spectroscopy. Spherical gold nanoparticles (isotropic) only have one absorption maxima at around 520 nm. It is more complicated for gold nanorods

(anisotropic) since they display two absorption maxima since there are oscillations along both the short or long axis (Figure 1.1[6]): one for the short axis (transverse band), one for long axis (longitudinal band). Aspect ratio (length/width) is controllable synthetically, which makes the longitudinal absorption maxima ranges from visible to near IR.

1.2 Tuning the size and shape

With more studies done on exploring nanoparticles, the methods of synthesizing gold nanoparticles (Au NPs) have been much more mature, which makes it possible to synthesize Au NPs in different sizes and shapes as desired. When dispersed in water, the color of Au NPs solution is shape-dependent. As the aspect ratio increase, the LSPR wavelength maximum (λ_{max}) increase (Figure 1.2a). Gold nanospheres (aspect ratio=1) exhibit a red color when suspended in water, and for elongated nanorods, colors like blue, green, and brown colors are observed (Figure 1.2b).

The properties of the Au NPs can be further tuned by altering surface chemistry, which can be achieved by coating through electrostatic or covalent interactions. Cationic cetyltrimethylammonium bromide (CTAB) bilayer coated gold nanorods and anionic citrate capped gold nanospheres are normally functionalized through layer-by-layer polyelectrolyte coating. Gold surfaces are also readily tuned by adsorption of thiols. By tuning surface chemistry, Au NPs are given different surface charges and additional functionalities. For example, as a toxic reagent, CTAB coated Au NPs are not suitable for biological studies, yet after replacing it with thiolated methoxypolyethylene glycol (mPEG), the cytotoxicity decreased[7].

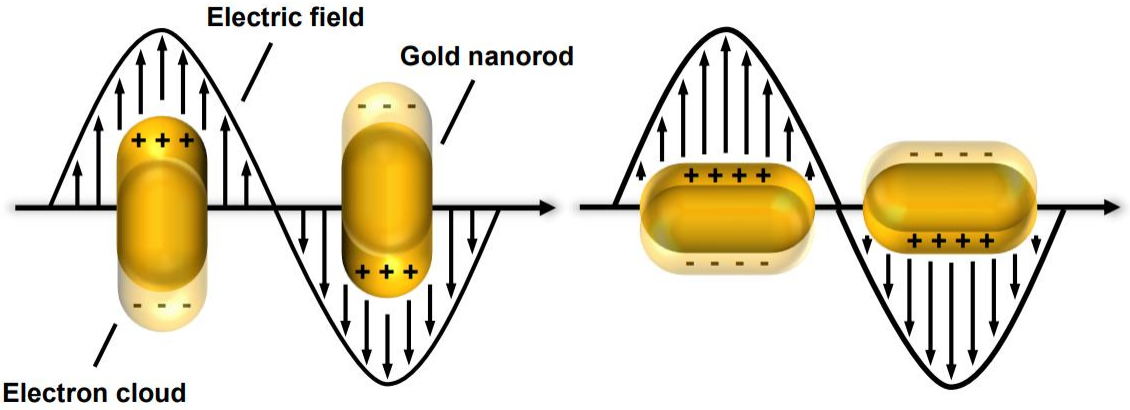

Figure 1. 1. Oscillations of conduction band electrons along the short and long axes result in two extinction maxima for gold nanorods. Adapted from ref 6. Copyrights 2019 Nardine S. Abadeer.

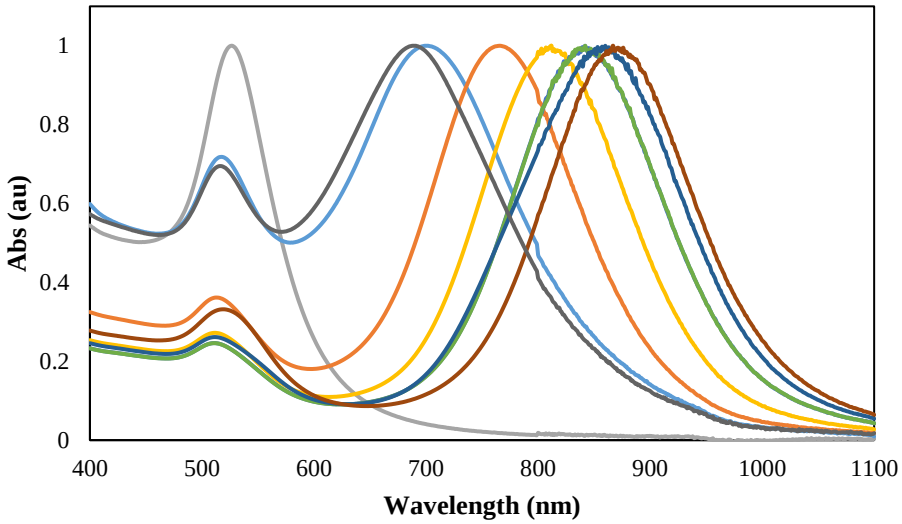

(a)

(b)

Figure 1.2. (a) A UV- vis absorption spectrum for Au NPs in water with different aspect ratios. The longitudinal λ_{max} increases with aspect ratio. (b) A picture of Au NP solution with an increased aspect ratio from left to right.

1.3 Synthesis of Au NPs

The "boiling citrate method" is the most utilized method to synthesis gold nanospheres and only three reagents are needed for this method: Gold (III) chloride trihydrate ($HAuCl_4 \cdot 3H_2O$), sodium citrate and water. After dissolving gold (III) chloride trihydrate in water and brought to boil, citrate is added. Citrate does not only serves as a reducing agent but also stabilizes gold nanospheres[8,9]. The size of the gold nanosphere can be controlled by modifying citrate concentration and reaction time[10]. However, this method can only produce gold nanospheres ranging from 12 nm to 40 nm in diameter. Larger gold nanospheres can be synthesized using a seed-mediated synthesis with hydroquinone as the reducing agent, which gives gold nanospheres as large as 200 nm[11].

The most commonly used method of gold nanorod synthesis is also seed-mediated[12]. The seeds are made from reducing $HAuCl_4 \cdot 3H_2O$ with sodium borohydride ($NaBH_4$). Seeds continue to grow in a solution of $HAuCl_4 \cdot 3H_2O$, CTAB, ascorbic acid, and silver nitrate ($AgNO_3$). The aspect ratio of the gold nanorods can be tuned by the amount of silver salt added to the reaction.

1.4 Characterization of Au NPs

The Murphy group, along with other groups, have been exploring and developing methods to synthesize Au NPs, aiming for better control of the size and the shape while increasing the yield. Characterization is an important step in this process.

UV-vis absorbance spectroscopy is one of the most used characterization techniques, which can be used for the identification of the location of the transverse and longitudinal LSPR. These two locations can be used to determine the size and aspect ratio of the nanorods, which can also be used the monitor the aggregation of Au NPs in general[12,13]. A narrow peak is an indication

of a monodisperse sample while the broadening of the peak is a sign of aggregation[14]. Another important application of the UV-vis spectroscope is to determine the concentration of the Au NPs concentration.

Dynamic light scattering (DLS) is another commonly used technique that is used to determine the size and size distribution of nanoparticles in solution. Moreover, the hydrodynamic diameter measured by DLS allows us to measure the size of the nanoparticles with the polyelectrolyte coating. Nanorods are observed as nanospheres and an average diameter will be reported. Zeta potential is another important characterization step which is usually measured by the same instrument as DLS. Zeta potential is a measure of the surface charge of the nanoparticles. A. electrode is placed in the sample and nanoparticles will move according to the electric field created by the electrode[15]. Zeta potential is calculated by the velocity of the nanoparticles' movement in the DLS instrument.

As a metal with high Z value, gold nanoparticles can scatter electrons. This property allows Au NPs to be characterized by electron microscopy such as transmission electron microscopy. The unscattered electrons pass through the sample and are collected by the detector which leaves a brighter region. Those electrons that get scattered by Au NPs will not be detected. TEM is a great technique to visualize the Au NPs which can be used to determine the exact size of the nanoparticles and, in some cases, the thickness of the polyelectrolyte coating[16,17].

1.5 Protein corona formation on gold nanoparticles

With more and more attention drawn to the biological use of Au NPs, the interaction between Au NPs and biological molecules is a crucial area to be explored. Many biomolecules,

proteins, in particular, undergo structural changes when interacting with Au NPs on the surface. This interaction is likely to disrupt the function of the protein by altering the native conformation.

When introduced in a biological system, proteins bind to the nanoparticle surface forming a dynamic structure called the protein corona. With the formation of the protein corona, the nanoparticles gain stability and biological properties that the particle alone didn't have. It's been hypothesized that the protein corona consists of two parts: a hard shell that is irreversibly bound to the nanoparticle and a secondary layer that reversibly interchange with other components from the biological system[18].

Many measurements are used to infer protein conformation and orientation on nanoparticles. Circular dichroism absorption spectroscopy (CD) is used to detect the conformation change of proteins. The native conformation of proteins contains structures such as α-helix and β-sheets, which have signature signals in CD spectra. The absence of these signals is a sign of disruption of proteins' native structures and binding to the surface of the Au NPs[19]. NMR is another technique for identifying the orientation and the binding site of proteins[20]. Matrix-assisted laser desorption/ionization (MALDI) mass spectrometry is also commonly used. After protein digestion, the fragments are analyzed, which give information about the orientation of the protein and its binding sites[21]. DLS gives information about the hydrodynamic diameter increase with the formation of protein corona and the number of proteins on the surface. The binding constant of protein is another parameter for the characterization of the protein corona, which describes the affinity of the protein to Au NPs. One analytical method to extrapolate binding constant is to expose gold nanoparticles to a protein sample with known concentration and measure the concentration of free protein left in the solution after the formation of the protein corona. This can be achieved by steady-state fluorescence quenching measurements, as gold quenches fluorophores

when the fluorophores are close to the gold nanoparticle surfaces[22]. The protein BSA with a fluorescein tag was incubated with gold nanoparticles to form the protein corona, which brought the fluorescein in proximity to the gold surface. With the Au NPs quenching the fluorescence, the only signal that can be detected was from free BSA. The rates of the association and dissociation of protein from nanoparticles provide information about the affinity between protein and nanoparticles. Techniques like surface plasmon resonance (SPR), isothermal titration calorimetry (ITC), and size exclusion chromatography were involved in obtaining the rate constants[23].

The binding constant of proteins and nanoparticles can be influenced by many facts, such as the surface chemistry, the size/ shape of Au NPs, the structure of the protein, and pH/ temperature/ ionic strength of the solution. According to Wangoo et al[24], the binding constants of BSA and IgG binding to the gold nanosphere were compared. Gold nanospheres that were 40 nm in size were synthesized by reducing tetrachloroauric acid with glutamic acid under refluxing. The binding constant of BSA and IgG to these gold nanospheres was $3.16\times 10^{11}M^{-1}$ and $1.82 \times 10^{12}M^{-1}$ respectively. From work done by the Murphy group[25], the binding constant of BSA to Au NPs with different aspect ratio and surface chemistry were calculated. The binding constant of BSA to CTAB coating particles are displayed in Table 1.1.

1.6 Biological application of Au NPs

Au NPs' capacity in the biological field has been explored for years and they are used for labeling, imaging, delivery, and disease treatment[26].

Due to the unique physical properties (size, shape, surface area), optical properties, biocompatibility, Au NPs have been researched greatly to be applied to biological or medical uses. Au NPs have decent stabilities when surrounded by biomolecules such as proteins and

Table 1.1. Binding constant of BSA to Au NPs with different aspect ratio and surface chemistry.

	Nanospheres			**Nanorods AR=3.5**			**Nanorods AR=18**		
	PAA	PAH	PEG	PAA	PAH	PEG	PAA	PAH	PEG
K_a ($\times 10^{10}$ M^{-1})	0.3±0.04	1.71±0.33	0.28±0.01	0.95±0.09	1.48±0.25	0.51±0.02	1.22±0.08	2.75±0.49	0.82±0.54

oligonucleotides. The presence of thiol functional groups in some biomolecules contributes greatly to the stability of the interaction be between Au NPs and these biomolecules and leads to higher stability of Au NPs. Imaging, drug delivery, diagnosis and therapy for cancer are examples for common uses for Au NPs

There are plenty of techniques that can be used to detect Au NPs: traditional like TEM due to the high Z value of gold; optical microscope due to the scatter of light and photoacoustic imaging due to the photothermal effect. These are the techniques that give Au NPs possibilities to be applied to imaging. One of the traditional application is immunostaining. Immunostaining, in essence, is the conjugation of an antibody that recognizes a specific molecule to Au NPs. It can be applied to fixed cells. Au NPs-antibody hybrid enters the fixed cells through the permeable membrane and accumulates at where the specific molecules are. This way the localization of a molecule can be achieved within cells. Immunostaining can also be applied to track the movement of cells. Au NPs are first functionalized with antibodies that recognize membrane proteins from the cells of interest and incubate with cells. The movement of the cells can be monitored by tracking the 'gold tag' on the surface of the membrane[29].

Photothermal cancer therapy is also a hot application. Traditional treatments have their limitations. The surgical removal of tumors is restricted by the size and location, and the chance of metastasis remains high. Chemotherapy is another commonly used cancer treatment, but it comes with intense side effects. However, photothermal cancer therapy can avoid this limitation. The idea behind photothermal therapy is that Au NPs can be heated up by visible to near IR light and the increase in temperature is lethal to cells. It has been confirmed that SK-BR-3 cancer cells can be terminated with photothermal cancer therapy, both in vitro and in vivo. The in vitro study was done by adding Au NPs suspension to the cell culture and exposed to near IR laser overnight.

With the radiation of laser, cells with Au NPs were killed. With the immune label on the surface of the particles, the specificity increase and left healthy cells unharmed. The accumulation Au NPs at the tumor site can kill cancer cells but also strengthen the uptake within the tissue[30].

1.7 References

1. Murphy, C. J.; Gole, A. M.; Stone, J. W.; Sisco, P. N.; Alkilany, A. M.; Goldsmith, E. C.; Baxter, S. C. Gold nanoparticles in biology: beyond toxicity to cellular imaging. *Acc. Chem. Res*. **2008**, 41 (12), 1721-1730.
2. Choi, J.; Yang, J.; Park, J.; Kim, E.; Suh, J.; Huh, Y.; Haam, S. Specific near-IR absorption imaging of glioblastomas using intergrin-targeting gold nanorods. *Adv. Funct. Mater*. **2011**, 21 (6), 1082-1088.
3. Nutting, J., and J. L. Nuttall. The malleability of gold. *Gold Bulletin*. **1977**. 10 (1), 2-8
4. Freestone, Ian, Nigel Meeks, Margaret Sax, and Catherine Higgitt. " the Lycurgus cup—a roman nanotechnology. *Gold bulletin*. **2007**. 40(4), 270-277.
5. Sui M, Kunwar S, Pandey P, Lee J. Strongly confined localized surface plasmon resonance (LSPR) bands of Pt, AgPt, AgAuPt nanoparticles. *Scientific reports*. **2019**, 9(1):1-4.
6. Abadeer, N. Harnessing the optical properties of gold nanorods: fluorescence enhancement, biosensing and photothermal therapy. Thesis. **2016**. University of Illinois at Urbana Champaign.
7. Niidome, T.; Yamagata, M.; Okamoto, Y.; Akiyama, Y.; Takahashi, H.; Kawano, T.; Katayama, Y.; Niidome, Y. Modification of Gold Nanorods Using Phosphatidylcholine to Reduce Cytotoxicity. *J. Controlled Release* **2006**, *114*, 343 – 347.
8. Biggs, S.; Chow, M. K.; Zukoski, C. F.; Grieser, F. The Role of Colloidal Stability in the Formation of Gold Sols. *J. Colloid Interface Sci.* **1993**, *160*, 511 – 513.
9. Biggs, S.; Mulvaney, P.; Zukoski, C. F.; Grieser, F. Study of Anion Adsorption at the Gold-Aqueous Solution Interface by Atomic Force Microscopy. *J. Am. Chem. Soc.* **1994**, *116*, 9150 – 9157.
10. Frens, G. Controlled Nucleation for the Regulation of the Particle Size in Monodisperse Gold Suspensions. *Nature* **1973**, *241*, 20 – 22.
11. Perrault, S. D.; Chan, W. C. W. Synthesis and Surface Modification of Highly Monodispersed, Spherical Gold Nanoparticles of 50-200 nm. *J. Am. Chem. Soc.* **2009**, *131*, 17042 – 17043.
12. Jana NR, Gearheart L, Murphy CJ. Wet chemical synthesis of high aspect ratio cylindrical gold nanorods. *J. Phys. Chem. B.* **2001**. 105(19):4065-7.
13. Ma, Z.; Tian, L.; Wang, T.; Wang, C. Optical DNA Detection Based on Gold Nanorods Aggregation. *Anal. Chim, Acta*. **2010**, 673, 179-184.
14. Gole, A.; Murphy, C. J. Biotin-Streptavidin-Induced Aggregation of Gold Nanorods: Tuning Rod-Rod. *Orientation. Langmuir*. **2005**, 21, 10756-10762.
15. Xu, R. Progress in Nanoparticles Characterization: Sizing and Zeta Potential Measurement. *Particuology*, **2008**, 6, 112-115.
16. Wang, Z. L. Transmission Electron Microscopy of Shape-Controlled Nanocrystals and Their Assemblies. *J. Phys. Chem. B.* **2000**, 104, 1153-1175.
17. Flannigan, D. J.; Zewail, A. H. 4D Electron Microscopy: Principles and Applications. *Acc. Chem. Res*. **2012**, 45, 1828-1839
18. Milani S, Baldelli Bombelli F, Pitek AS, Dawson KA, Radler J. Reversible versus irreversible binding of transferrin to polystyrene nanoparticles: soft and hard corona. *ACS nano*. **2012**. 6(3):2532-41.
19. Linse, S.; Cabaleiro-Lago, C.; Xue, W.-F.; Lynch, I.; Lindman, S.; Thulin, E.; Radford, S. E.; Dawson, K. A. Nucleation of Protein Fibrillation by Nanoparticles. *Proc. Natl. Acad. Sci.* **2007**, *104*, 8691 – 8696.

20. Calzolai, L.; Franchini, F.; Gilliland, D.; Rossi, F. Protein−Nanoparticle Interaction: Identification of the Ubiquitin−Gold Nanoparticle Interaction Site. *Nano Lett.* **2010**, *10*, 3101−3105.
21. Shrivastava, S.; Nuffer, J. H.; Siegel, R. W.; Dordick, J. S. Position-Specific Chemical Modification and Quantitative Proteomics Disclose Protein Orientation Adsorbed on Silica Nanoparticles. *Nano Lett.* **2012**, *12*, 1583−1587.
23. Cedervall T, Lynch I, Lindman S, Berggård T, Thulin E, Nilsson H, Dawson KA, Linse S. Understanding the nanoparticle–protein corona using methods to quantify exchange rates and affinities of proteins for nanoparticles. *Proceedings of the National Academy of Sciences*. **2007**. 104(7):2050-5.
24. Wangoo N, Suri CR, Shekhawat G. Interaction of gold nanoparticles with protein: a spectroscopic study to monitor protein conformational changes. *Applied Physics Letters*. **2008**. 92(13):133104.
25. Boulos SP, Davis TA, Yang JA, Lohse SE, Alkilany AM, Holland LA, Murphy CJ. Nanoparticle–protein interactions: a thermodynamic and kinetic study of the adsorption of bovine serum albumin to gold nanoparticle surfaces. *Langmuir*. **2013**. 29(48):14984-96.
26. Sperling, R. A.; Rivera Gil, P.; Zhang, F.; Zanella, M.; Parak, W. J. Biological Applications of Gold Nanoparticles. *Chem. Soc. Rev*. **2008**, 37, 1896-1908.
27. Murphy, C. J.; Gole, A. M.; Stone, J. W.; Sisco, P. N.; Alkilany, A. M.; Goldsmith, E. C.; Baxter, S. C. Gold Nanoparticles in Biology: Beyond Toxicity to Cellular Imaging. *Acc. Chem. Res*. **2008**, 41, 1721-1730.
28. Sasidharan, A.; Monteiro-Riviere, N. A. Biomedical Applications of Gold Nanomaterials: Opportunities and Challenges. *Wiley Interdiscip. Rev. Nanomed. Nanobiotechnol*. **2015**, 7, 779-796.
29. Sperling RA, Gil PR, Zhang F, Zanella M, Parak WJ. Biological applications of gold nanoparticles. Chem. Soc. Rev. 2008. (9):1896-908.
30. Lowery AR, Gobin AM, Day ES, Halas NJ, West JL. Immunonanoshells for targeted photothermal ablation of tumor cells. Int. J. Nanomedicine. 2006. (2):149.

CHAPTER 2: Cellular Motion: Chemotaxis

2.1 Introduction to chemotaxis

Chemotaxis is a special type of directional cell movement along the gradients of molecules, called chemoattractant. Chemotaxis is a widely present phenomenon that exists in eukaryotic cells and prokaryotic cells such as bacteria. An example of chemotaxis is that the bacteria *Escherichia coli* is attracted to serine and aspartic acid; slime mold responds to cAMP and leucocytes move towards serum factors[1]. Even though the movement of cells or bacteria had been observed as early as the invention of the optical microscope, the phenomenon 'chemotaxis' didn't come to existence until 1881. It was first found by Dr. Theodor Wilhelm Engelmann, who was a German microbiologist. The movement of bacteria towards chloroplast in the presence of *Spirogyr*a algae caught his attention then he hypothesized that the bacteria was moving directionally towards the algae, the source of oxygen. This hypothesis was confirmed by his experiments conducted in 1882. A specialized microscope was used which was able to visualize the concentration of oxygen. As expected, the bacteria was moving directionally up the gradient of oxygen[2].

Chemotaxis is heavily involved in processes such as cancer metastasis, immune response, wounding healing, and embryogenesis[3-6]. During embryogenesis, chemotaxis is involved in forming and organizing tissues and the nervous system. During immune responses, leukocytes are recruited to the site of inflammation directs by chemoattractants[7]. Understanding the fascinating mechanism behind chemotaxis might be a crucial step to stop cancer metastasis.

The driving force of eukaryotic cell movement is the polymerization of actin (Figure 2.1). With the actin polymerize and extend, cells are 'pushed' forward. For chemotactic cells, they not only can sense the signal but also the direction of it. The growth of actin filament starts to

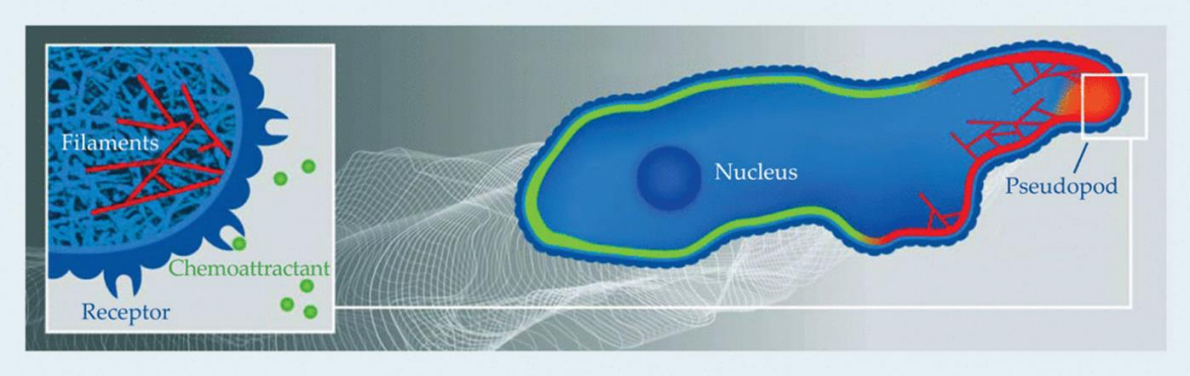

Figure 2.1. Simple mechanism of chemotaxis. Adapted from ref 11. Copyright 2013 American Institute of Physics.

polymerize when the asymmetric stimuli are applied. When cells start to react to the asymmetric stimuli, they are

polarized. Polarized is not restricted to describe the asymmetric shape of the cell, but also the uneven sensitivity between the 'front' and 'back' of the cells. With higher sensitivity in the front, where cells are exposed to higher concentrations, cells are made sure to move along the gradient. It was also observed that actin and actin-binding proteins started to accumulate when cells are polarized[8]. Chemoattractant receptors were found on the surface of chemotactic cells. One type of amoebae was noticed to move towards cAMP when they starved, and four types of receptors were located on the surface, which is coupled to a G protein. Surprisingly, 20 chemoattractant receptors were found that are coupled with the same G protein[9,10]. This explains well why the chemoattractant gradient needs to be 'delicate', a slightly too high a concentration can lead to numbness of cells due to the oversaturation of the chemoattractant receptors. The polarization process is not identical to all cells. Some cells remain static until the activation of the chemoattractant, while some other cells move freely until they sense the gradient.

2.2 Approaches to understanding chemotaxis

Since the discovery of chemotaxis, many approaches have been developed. One of the most popular assays is with Boyden Chamber (Figure 2.2). Boyden chamber was invented by D. Stephen Boyden to analyze the chemotaxis of leukocytes. The setup is that two chambers filled with media are separated with a membrane. Chemoattractant is added to the bottom and diffuses to form the gradient, while cells from the top would react to the gradient and travel through the membrane. After a period of incubation, cells are fixed and stained. The number of cells that traveled through the membrane can be used to evaluate the chemotactic effect[12].

With the development of scientific technology, tools, and methods used to study chemotaxis have been more convenient and efficient than before. The movement of every single cell can be tracked over time. Important data such as velocity and accumulated path length can be extrapolated easily. Statistical analysis is applied and several parameters[13] can be used to describe the chemotactic interaction between cells and chemoattractants.

The Center of mass (Figure 2.3) is the spatial average of all the cells. It is normally displayed in a form of coordinates. The starting center of mass is set to zero and the coordinate is the average of all the endpoints. It can be either positive or negative depending on the direction of the movement. When chemoattractant is applied, the center of mass would shift towards the source of chemoattractant. The distance between the starting and the end center of mass is referred to as displacement, and it is normally considered as the distance traveled by cells as a group.

Directness (D) the ratio of Euclidian distance over the accumulated distance traveled by cells. D is a none-zero value between 0 and 1 (Figure 2.4). When D=1, then Euclidian distance equals the accumulated distance and the path that the cell traveled was a straight line. So directness is a way to describe how straight the migration is. Directness is relative, as there is not a critical value for directness to tell whether there is a chemotactic effect.

Forward migration index (FMI) is the most important parameter for evaluating the chemotactic effect. It is the ratio between the projection on the x and y-axis over the accumulated distance and it is a good indication of the efficiency of the movement (Figure 2.5). It can be either positive or negative depending on the direction. Thus there are FMI_x and FMI_y and sometimes refer as $FMI_{\perp}$ and $FMI_{/\!/}$. Normally the x-axis is where the gradient lies. When the chemoattractant is applied, cells will move directionally along axes. This would result in a nearly zero FMI_y and a much larger FMI_x.

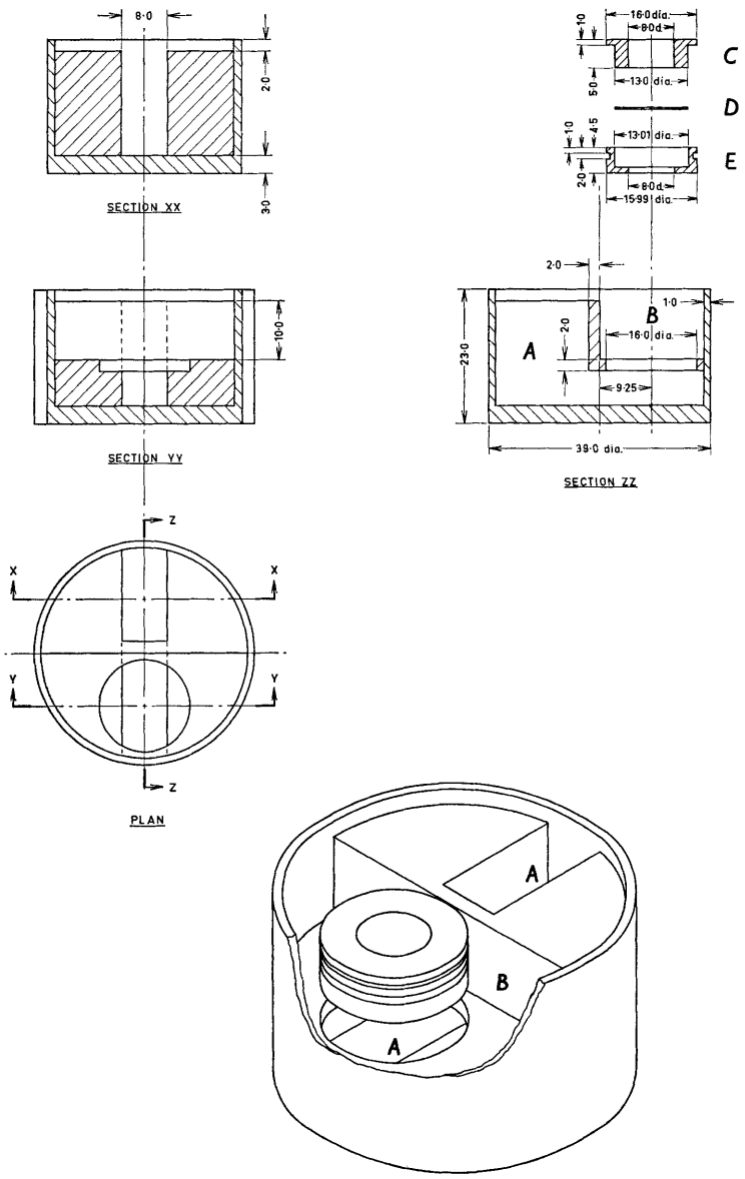

Figure 2.2. Structure of the Boyden Chamber. Adapted from ref 14. Copyright 1962 Rockefeller University Press.

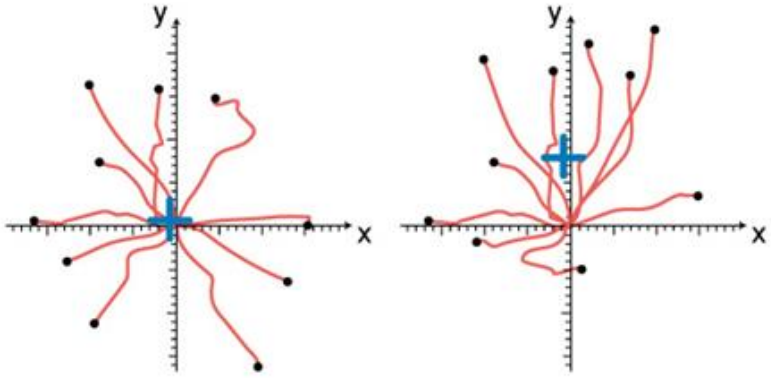

Figure 2.3. An example of a group of cells move along the y-axis positive direction. The blue cross represents the center of mass. Adapted from ref 13. Copyright 2013 Ibidi GmbH

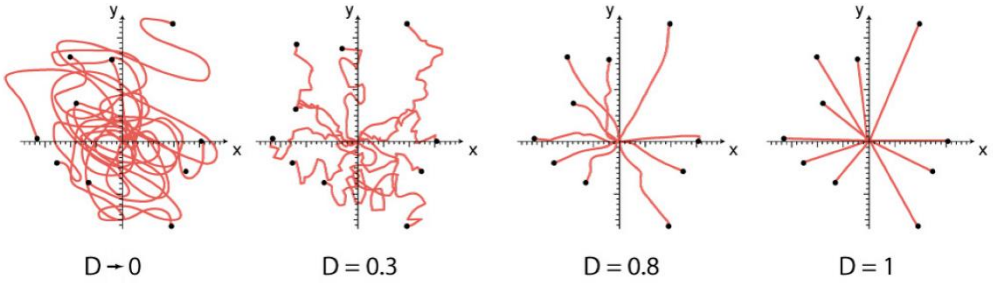

Figure 2.4. Example of migration paths with different D values. With a directness closer to 1, the path is more linear. Adapted from ref 13. Copyright 2013 Ibidi GmbH.

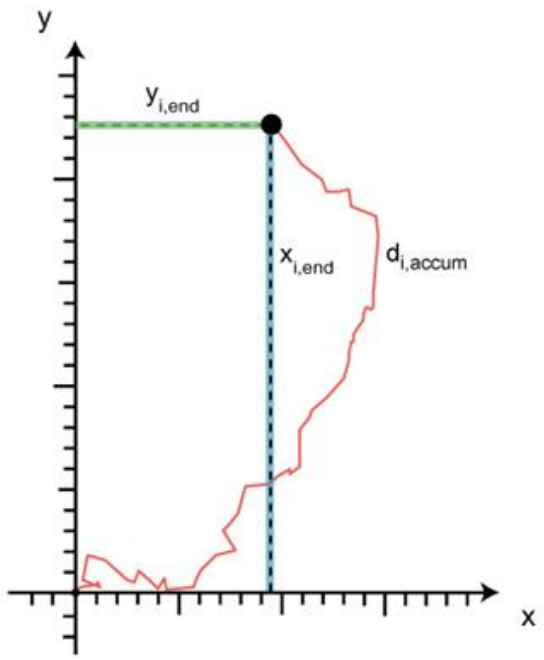

Figure 2.5. An indication of how FMI is calculated. FMI is the ratio of x_i/y_i over d^{accum}. Adapted from ref 13. Copyright 2013 Ibidi GmbH.

Rayleigh test (p-value) is a statistical test for uniformity of the radial distribution of endpoints. A low p-value points to a non-homogenous distribution (Figure 2.6). The critical value for the p-value is 0.05, which means if a p-value larger than 0.05 the population is homogeneous. When a chemoattractant is applied, the cell population will lose its homogeneity and result in a low p-value.

2. 3 Examples of chemotaxis pairs

Many chemotaxis pairs have been well studied and used as models for new researches.

As the organism that is involved in the very first chemotaxis study, *Escherichia coli* is one of the most well-studied models for chemotaxis. Unlike most other cells that go through chemotaxis, *E. coli*'s size (around two microns) is too small that it is not able to detect the concentration difference around its body. Instead, it seems to have 'memory' of the chemical environment. There are two types of movements involved in chemotactic motion, *E. coli* can either 'run' or 'tumble'. With the presence of chemoattractant, it behaves just like any other chemotactic cells. However, if it is moving away from chemoattractant or getting closer and closer towards chemorepellent, it tends to tumble and turn around. Common chemoattractants for E. coli are amino acid, sugars, pyrimidine, and electron acceptors such as oxygen and potentially toxic chemicals such as phenol, alcohol and fatty acids are examples of chemorepellents. The receptor complexes for bacteria chemotaxis are sometimes considered as 'nanobrain' due to their ability to process information that they sense then control their movement[15].

The neutrophil is another commonly used model for chemotaxis research. 40% to 70% of white blood cells are neutrophils and they plan an important role in the innate immune system. They exist in the bloodstream and are recruited to the site of inflammation. Chemoattractants

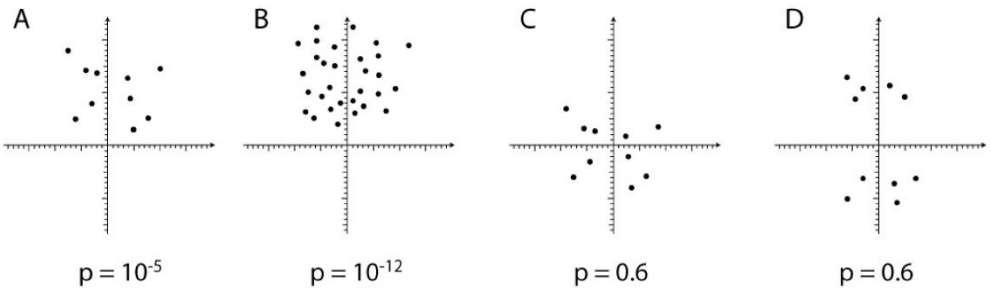

Figure 2.6. Populations with a different p-value. With a $p<0.05$, the distribution is non-homogeneous. Adapted from ref 13. Copyright 2013 Ibidi GmbH.

gradient lead them through the blood vessels and interstitial tissues. N-Formylmethionyl-leucyl-phenylalanine (fMLF)[16] and Interleukin 8 (IL-8) are the two most popular chemoattractants for neutrophil. fMLF belongs to a family called N-formyl peptides, which are potent chemoattractants for while blood cells. It is originally synthesized and secreted by bacteria. Neutrophils chase bacteria by following the fMLF gradient to arrive at the inflammation site. Genes coding for N-formyl peptides are located in mitochondria and chloroplasts and they are activated when inflammation happens, to recruit white blood cells more efficiently2. Unlike fMLF, IL-8 is generated by macrophages and cells like epithelial cells and muscle cells. Their functions are to attract neutrophils to the site of infection and stimulate phagocytosis. The synthesis and secretion of IL-8 start when bacteria are spotted by the macrophage. The positive feedback starts when high oxidant stress leads to higher IL-8 production, which leads to higher oxidant stress[17].

2.4 Reference

1. Schiffmann E, Corcoran BA, Wahl SM. N-formylmethionyl peptides as chemoattractants for leucocytes. *Proceedings of the National Academy of Sciences*. **1975**. 72(3):1059-62.
2. Engelmann TW. Ueber den faserigen Bau der contractilen Substanzen, mit besonderer Berücksichtigung der glatten und doppelt schräggestreiften Muskelfasern. *Archiv für die gesamte Physiologie des Menschen und der Tiere*. **1881**. 25(1):538-65.
3. Muller, A. et al. Involvement of chemokine receptors in breast cancer metastasis. *Nature*. **2002**. 410: 50–56.
4. Behar, T.N. et al. GABA-induced chemokinesis and NGF-induced chemotaxis of embryonic spinal cord neurons. *J. Neurosci*. **1994**. 14: 29–38.
5. Wilkinson, P.C. Chemotaxis and Inflammation. **1982**. Churchill Livingston, New York.
6. Condeelis JS, Wyckoff JB, Bailly M, Pestell R, Lawrence D, Backer J, Segall JE. Lamellipodia in invasion. *InSeminars in cancer biology*. **2001**. Academic Press.
7. Devreotes P, Janetopoulos C. Eukaryotic chemotaxis: distinctions between directional sensing and polarization. *J. Bio. Chem*. **2003**. 278(23):20445-8.
8. Iijima M, Huang YE, Devreotes P. Temporal and spatial regulation of chemotaxis. *Developmental cell*. **2002**. 3(4):469-78.
9. Klinker JF, Wenzel-Seifert K, Seifert R. G-protein-coupled receptors in HL-60 human leukemia cells. *General Pharmacology: The Vascular System*. **1996**. 27(1):33-54.
10. Murphy PM. The molecular biology of leukocyte chemoattractant receptors. *Annual review of immunology*. **1994**. 12(1):593-633.
11. Levine H, Rappel WJ. The physics of eukaryotic chemotaxis. *Physics today*. **2013**. 66(2).
12. Chen HC. Boyden chamber assay. *In Cell migration*. **2005**. Humana Press.
13. Asano Y, Horn E. Instructions Chemotaxis and Migration Tool 2.0. **2013**
14. Boyden S. The chemotactic effect of mixtures of antibody and antigen on polymorphonuclear leucocytes. *J Exp Med*. **1962**.115(3):453-466.
15. Webre DJ, Wolanin PM, Stock JB. Bacterial chemotaxis. *Current Biology*. **2003**. 13(2):R47-9.
16. Panaro MA, Mitolo V. Cellular responses to FMLP challenging: a mini-review. Immunopharmacology and immunotoxicology. **199**9. 21(3):397-419.
17. Hedges JC, Singer CA, Gerthoffer WT. Mitogen-activated protein kinases regulate cytokine gene expression in human airway myocytes. *AM. J. RESP. CELL. MOL*. **2000**. 23(1):86-94.

CHAPTER 3: Do Gold Nanoparticles Interfere with Chemotaxis?

3.1 Introduction

It has been reported that colloidal nanoparticles can cause cells to undergo phenotypical and behavioral changes[1-6]. Studies have been done on cell migration with the treatment of gold nanoparticles. Previous works done in our lab showed that cells would actively pick up gold nanoparticles while moving, and later we found out that uptake or even interaction with gold particles was not required to influence cell migration pattern. However, the mechanism of how gold nanoparticles are involved in cell migration is not fully understood[7-15].

Chemotaxis is the migration of cells and small organisms in the response of chemical gradient[16]. This phenomenon exists commonly in nature, such as the movement of bacterial away from phenol and towards glucose; leukocytes move towards the site of infection or injury[17]. It's also believed to be the mechanism involved in cancer metastasis[18]. These observations make studying chemotaxis important, which provides insight to improve vaccination and reduce cancer metastasis. The chemicals that are involved in chemotaxis are called chemoattractants. A good example of a chemotactic pair would be bacteria moving towards glucose (chemoattractant), and away from phenol (chemorepellents).

The purpose of this study is to understand the effect of gold nanoparticles on cell migration. A previous study has shown that proteins tend to interact with Au NPs depending on the size and surface chemistry[19-25]. The decrease in concentration is roughly in the nanomolar range. Chemotaxis can happen with gradients that are only 0.5% change in concentration over the length of the cell, which is extremely sensitive[26]. With this sensitivity, the loss of bioavalibity of chemoattractant by interaction with Au NPs can cause cell behavior to alter.

Two systems were closely were studied. One was a human monocytic cell line THP-1, which was derived from an acute leukemia patient. Monocytes are a type of white blood cells and they are heavily involved in immune responses. Their functions are regulated by chemotaxis by sensing chemoattractant secreted by other cells. There are three main types of chemoattractants: monocyte chemotactic protein, arachidonic acid metabolites, and N-formyl peptides. N-formyl-Nle-Leu-Phe-Nle-Tyr-Lys was chosen as the chemoattractant[27]. Another cell/molecule pair is human dermal fibroblast (HDF) with platelet-derived growth factor (PDGF) [28,29]. HDF cells are responsible for closing up wounds and producing connective tissues and they are recruited to the wound site by chemoattractants such as PDGF. PDGF is a family of protein that plays important role in blood vessel formation and the migration of mesenchymal cells and it is a dimeric glycoprotein that is composed of two subunit A or two subunits B, or one of each. In our study we used PDGF-BB. HDF is responsible for generating connective tissue and wound recovery, and as a type of mesenchymal cells, it responses to PDGF concentration.

3.2 Materials and methods

3.2.1 Materials

Gold (III) chloride trihydrate (HAuCl4 • 3H2O, ⩾ 99.9%), sodium citrate tribasic dehydrate ($Na_3Ct \cdot 2H_2O$, ⩾99%), hydroquinone (⩾99%), poly (sodium 4-styrenesulfonate) (PSS, M.W. ~70,000), poly(diallyldimethylammonium chloride) solution (PDADMAC, M.W. <100,000, 35 wt. % in H2O) were obtained from Sigma Aldrich. The fluoresceinated N-formyl peptide was obtained from ThermoFisher.

Human dermal fibroblast (HDF) and THP-1 cells were obtained from ATCC. HDF medium was high glucose DMEM with 1mM sodium pyruvate Mediatech 50003, 3.7g/L sodium

bicarbonate with 10% FBS and 1% pen-strep. THP-1 medium was RPMI 1640 medium with 2 mM L-glutamine, 1.5 g/L sodium bicarbonate, 4.5 g/L glucose, 10 mM HEPES and 1.0 mM sodium pyruvate, 0.05 mM 2-mercaptoethanol, 10% FBS and 1% pen-strep.

Poly electrolytes were 10 mg/mL in 1 mM NaCl solution. Ultrapure deionized water was used.

3.2.2 Methods

3.2.2.1 Synthesis of gold nanospheres

Gold nanoparticles with 80nm in size were synthesized[30]. Seeds were synthesized first. 0.5 mL of 1% HAuCl4 was added to 200 mL nanopure water. The reaction was heated to boil. 5 mL of 1% sodium citrate was added to the boiling solution. The temperature is lowered to 210^{o}C to keep the reaction boiling for 40 min. The heat was turned down and the reaction was set aside to cool to room temperature. 1 mL of 1% sodium citrate was added to the solution. The solution showed a dark red color. Seeds were purified by centrifugation at 12,000 xg for 20 minutes. The supernatant was removed and seeds were resuspended in 5 mL nanopure water. 5 mL of 1% HAuCl4 was added to 475 mL of nanopure water. 0.142 mL of seed solutions were then added to the solution. 1. 1 mL of 1% sodium citrate was added, followed by 5 mL of 0.03 M of hydroquinone. The solution turns opaque instantly and further stirred at room temperature for 60 min. The gold nanoparticles were purified by centrifugation at 5,000 xg for 20 minutes. The supernatant was removed and the gold nanoparticle pellet was collected. Particles were further wrapped with polyelectrolytes. PDADMAC, PSS was used for these large spheres to give different surface charges. Citrate Au NPs were purified with centrifugation then collected and resuspended in 1 mL water. 100 μL NaCl solution was added to Au NP solution followed by a 200 μL

polyelectrolyte solution and the solution was incubated overnight then purified by centrifugation. UV-vis, DLS, zeta-potential, and TEM were used to characterize these large spheres.

3.2.2.2 Chemotaxis assay for THP-1/ N-formyl peptide

THP-1 cells were first thawed in a water bath and cell solution was first transferred to 10 mL growth media. Cells were spun down with centrifuge and the supernatant was discarded to remove DMSO from the cell sample. The cell pellet was further resuspended with growth media and placed into a 50 mL flask. Cell culture was preserved in a 37 ^{o}C incubator with 5% CO_2. Growth media needs to be changed when cell number doubles, for THP-1 it's around two days. Cells were spun down and the supernatant was discarded. The cell pellet was then resuspended in fresh media and placed back to the flask. However, cells seemed inactive for the first two weeks. RPMI with 10% FBS was replaced by PRMI with 20% FBS to promote the growth of cells, and after treated for a week cells started to function normally. After cells can divide naturally, one to two million cells were centrifuged down and resuspended in growth media/ DMSO solution with a total volume of 1 mL, and preserved in a nitrogen tank for future use. N-formyl peptide came in with 1 mg peptide in a vial then dissolved in 1 mL PBS. The 1 mL solution was further divided into 20 working aliquots. Each working aliquot was preserved in -20 ^{o}C freezer until use. After removing from the freezer, the peptide solution can only be used for no more than three days.

Working aliquots of water, 3 mg/mL collagen, and HCO_3^- solution was prepared and stored in -4 ^{o}C and warmed up at room temperature right before use. Water bath should be avoided when warming up collagen, even though no visible change was observed, the Collagen that was warmed up in the water bath seemed to lose its ability to polymerize. Media MEM and RPMI along with the chemotaxis slide were pre-equilibrated in the incubator a day before the experiment. Cells were

centrifuged down and diluted so that in 50 μL suspension there are 18×10^6 cells. This concentration varies each time depending on whether cells were evenly distributed and whether cell clusters were broke apart. However, aiming for slightly higher concentration than the ideal concentration worked better for microscope observations. 20 μL MEM, 20 μL H_2O, 10 μL HCO_3^- (7.5%), 50 μL RPMI, 150 μL collagen (3mg/mL) and 50 μL cell suspension were added to a tube in this order and mixed well[31,32]. As soon as all the solutions were combined, a raise in its viscosity was observed. The mixture needed to be added to the channel gently within two minutes. It was recommended to incline the slide while adding a gel mixture so that bubbles can be pushed out from the top by the gel mixture. After the gel mixture was added to the channel, it was placed in an incubator for 45 min for collagen to polymerize. After the gel solidified, cell media was added to the right chamber while to the left chamber cell media with various concentrations of chemoattractants ware added.

Bright-field imaging was obtained with a Zeiss Observer Z1 microscope at 10X magnification. The time-lapse mode was used and images were taken every ten minutes for 24 hours. Micrographs were displayed in the Zen Blue software. Cell movements were tracked with ImageJ and plotted and analyzed with Cell Migration Tool from Ibidi. At least 20 cells were tracked for each experiment.

3.2.2.3 Chemotaxis assay for HDF/ PDGF

HDF cells were obtained from a liquid nitrogen tank and thawed in a water bath. The cell solution was first transferred to 10 mL growth media (DMEM) without serum (FBS). Cells solution was spun down with centrifuge and the supernatant was discarded to remove DMSO from the cell sample. The cell pellet was further resuspended with growth media (DMEM with FBS)

and placed into a 50 mL flask. Cell culture was preserved in a 37 ^{o}C incubator with 5% CO_2. HDF was spherical at first when transferred to the flask but after around six hours, cells started to attach to the bottom of the flask and became long and skinny. Cell media was changed twice per week. Since the FBS from the media contains the chemoattractant (PDGF) involved in the study, a specialized DMEM solution was made with 1% BSA instead of FBS. To remove the PDGF from the regular DMEM media, cells were treated with DMEM-BSA solution the day before experiments and were starved overnight. PDGF solution was obtained from our fridge. Each working aliquot contains 10 μL of 0.1 mg/mL of PDGF in water. It was further diluted in DMEM to 10 ng/mL, 20 ng/mL, 30 ng/mL, 40 ng/mL, 50 ng/mL, 60 ng/mL, 1 mL each. These PDGF working aliquots were preserved in -20 ^{o}C freezer, and during the experiment period, they can be temporarily stored in 4 ^{o}C fridge for no longer than three days.

Working aliquots of water, 1M NaOH solution, 3 mg/mL collagen, and HCO_3^- solution was prepared and stored in 4 ^{o}C and warmed up at room temperature right before use. A small amount of media 10X DMEM and DMEM-BSA along with the chemotaxis slide were pre-equilibrated in the incubator a day before the experiment. Since the regular DMEM media contains FBS, and the undefined PDGF concentration from serum makes it impossible to predict the gradient, the regular DMEM media was replaced by DMEM with 0.1% BSA. Cells were taken out and counted before preparing the cell mixture. After breaking apart cell clusters, one drop (~10 μL) of the cell solution was taken out and placed in a hemocytometer. Four squares were counted and averaged for approximating the total amount of cells in the solution. Normally each 50 mL flask gives around 2.5×10^6 cells at the confluence. After counting, the cell solution was centrifuged down and diluted so that in a 50 μL suspension contains 18×10^6 cells. With only 2.5×10^6 cells in one flask, it is very hard to get an accurate concentration of the cell due to the small

amount of media that's needed to dilute, and normally two flasks are combined for experiments. However, the concentration (18×10^6 cell/mL) from the protocol seemed slightly too high for HDF cells since after they settled in the gel matrix their size change and could overlap with each other. 1.6×10^6 cell/mL was the most ideal concentration for HDF. 20 μL DMEM, 6 μL NaOH 1M, 14 μL H_2O, 10 μL HCO_3^- (7.5%), 50 μL DMEM-BSA, 150 μL collagen (3mg/mL) and 50 μL cell suspension were added to a tube in this order and mixed well. The mixture should be cloudy without any visible cell clusters. The mixing process needs to be both gentle and quick since HDF were observed to form clusters very shortly after mixing. The mixture was added to the channel in the middle of the slide and placed in an incubator for 45 min for collagen to polymerize. After the polymerization, collagen fibers can be observed and cells would be trapped between those fibers and remain spherical. Cells were started to stretch with time and become more transparent. After the gel solidified within the channel, cell media was added to the right chamber while to the left chamber cell media with various concentrations of chemoattractant was added.

Bright-field imaging was obtained with a Zeiss Observer Z1 microscope at 10X magnification. The time-lapse mode was used and images were taken every ten minutes for 24 hours. Micrographs were displayed in the Zen Blue software. Cell movements were tracked with ImageJ and plotted and analyzed with Cell Migration Tool from ibidi. At least 20 cells were tracked for each experiment.

3.3 Instrumentation

Centrifuges were used during the synthesis and purification of Au NPs. Standard absorption spectra were measured with Cary 500 Scan UV-vis-NIR spectrophotometer. Dynamic light scattering measurements and zeta potential were measured with Malvern Zetasizer Nano S.

Brightfield imaging was performed on a Zeiss Observer Z1 microscope. Time-lapse images were recorded using multi-title time-series acquisition in the Zen Blue software at everything ten minutes for 24 hours.

3.4 Results

3.4.1 Characterization of Au NPs

To compare to previous studies, 80 nm gold nanospheres were chosen for this project. Au NPs with three different surface chemistry were synthesized and characterized with UV−vis spectroscopy, dynamic light scattering (DLS), and ζ potential.

With the increasing diameter during the coating process, UV-vis spectroscopy measurements indicated a slight red shift of ~3-4 nm in the wavelength (Figure 3.1). The diameter of each particle was further calculated based on the UV-vis measurements: citrate 69 nm, first layer PDADMAC 75nm, PSS 77 nm, and second layer PDADMAC 82 nm. Each layer of polyelectrolytes increases the diameter by 2 nm to 6 nm.

An increase of about 8-13 nm in the hydrodynamic size of the Au NPs was observed after functionalization (Figure 3.2 a). No aggregation appeared during measurements. Zeta potential measurements indicated changes in Au NP surface charges after the coating polyelectrolytes (Figure 3.2 b). Both the increase in hydrodynamic diameter and the changing of surface charge suggested the success of the functionalization of Au NP. All the characterization data are summarized in Table 3.1.

The visualization of Au NPs before polyelectrolyte coating was performed with cryo TEM imaging (Figure 3.3), and the average diameter of Au NPs was around 94.24 nm. There are

unknown coatings on the surface of the Au NPs. Even though the exact composition of the shell remains unclear, it is very similar to inorganic salt structure such as silica shell or metal-organic framework (MOF), which was likely due to the impurity from the synthesis. However, the redshifts on UV-vis spectra, the increase in hydrodynamic diameter, and changing in zeta potential all point to the assumption that the coating of Au NPs with polyelectrolytes did happen.

3.4.2. Detecting the chemotaxis of THP-1 with N-formyl peptide

The stability of the Au NP in the cell media RPMI was tested. Two methods were compared. The direct method involved the direct addition of the Au NPs into RPMI with 10% FBS while the sequential method dissolved Au NPs in RPMI with 20% FBS then further diluted FBS to achieve 10% FBS. Visible aggregation was observed with the direct method. However, with the sequential methods, high protein concentration from the FBS lead to the formation of the protein corona, which prevents Au NPs from aggregating. No obvious aggregation was observed from the sequential method (scheme 3.1).

3.4.3. Evaluate the chemotactic effect of THP-1 and N-formyl peptide

The ibidi μ-Slide Chemotaxis was used to observe the chemotactic effect (Scheme 3.2). Cells were seeded into the channel as part of the collagen gel mixture. With adding chemoattractant to the left reservoir, a linear gradient formed inside the gel along the x-axis. Cell movements were tracked for 24 hours. At least 20 cells were tracked. The starting points of cells were plotted at the origin and their trajectory paths overlapped to generate a 2D trajectory plot. 2 nM was chosen as the most ideal concentration according to literature[34-37] and concentrations around 2 nM were also tested to achieve the maximum movement for future studies (Figure 3.4b).

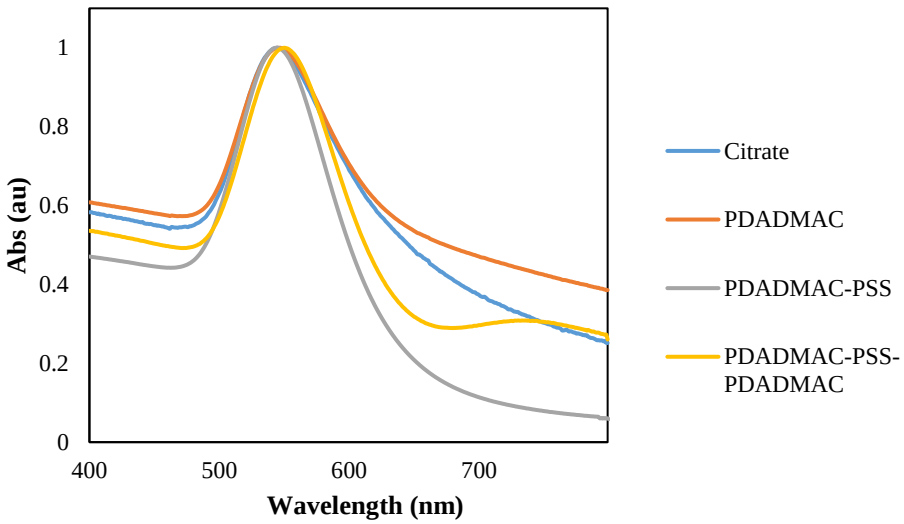

Figure 3.1. UV-vis spectra of Au NPs before and after functionalization, for three different surface chemistry. Each layer of polyelectrolyte gave a slight red shift of ~4 nm in wavelength.

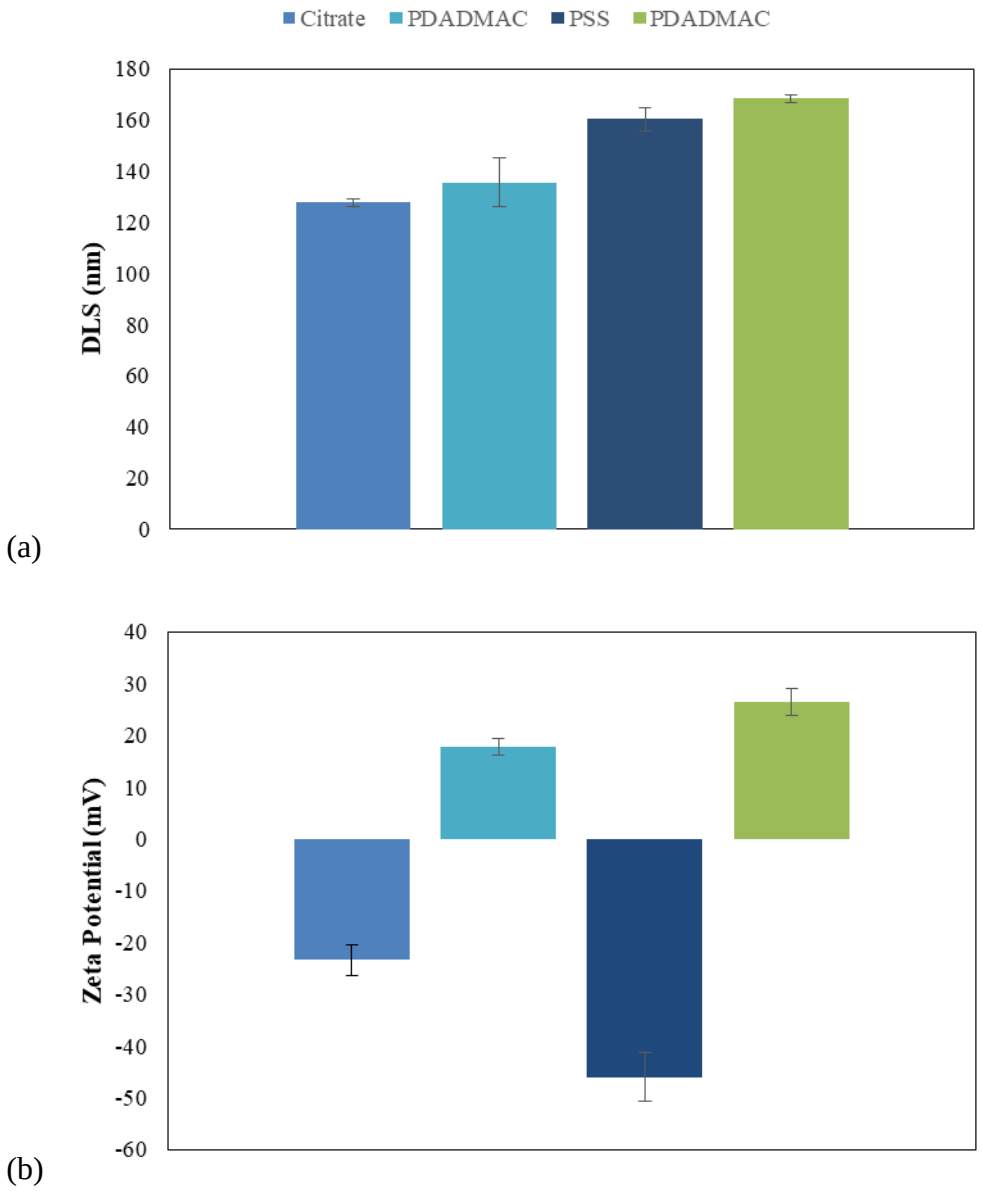

Figure 3.2. Hydrodynamic diameter (a) and zeta potential (b) of Au NP with different surface chemistry.

Table 3.1. The changes in hydrodynamic diameter and zeta potential after each functionalization.

Au NP	Citrate	PDADMAC	PDADMAC-PSS	PDADMAC-PSS-PDADMAC
d_h(nm)	127.7±1.5	135.6±1.5	160.3±9.4	168.5±4.35
ζ-potential (mV)	-23.4±2.9	17.8±1.6	-46.1±4.7	26.4±2.54

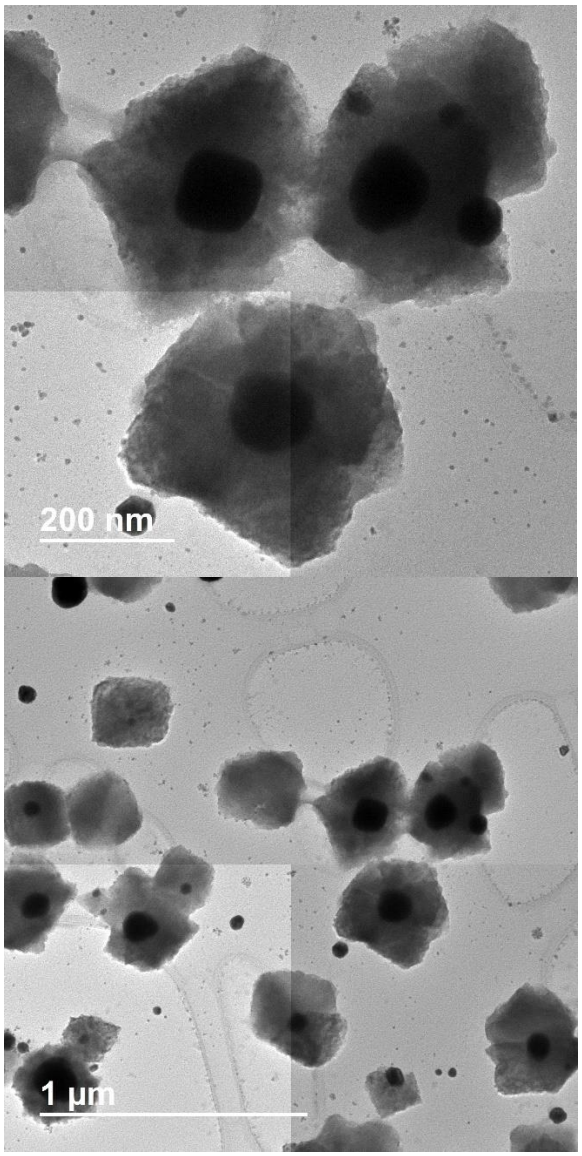

Figure 3.3. TEM image of citrate Au NPs without polyelectrolyte coating.

Scheme 3.1.[33] Introduction of Au NPs into cell media with two methods.

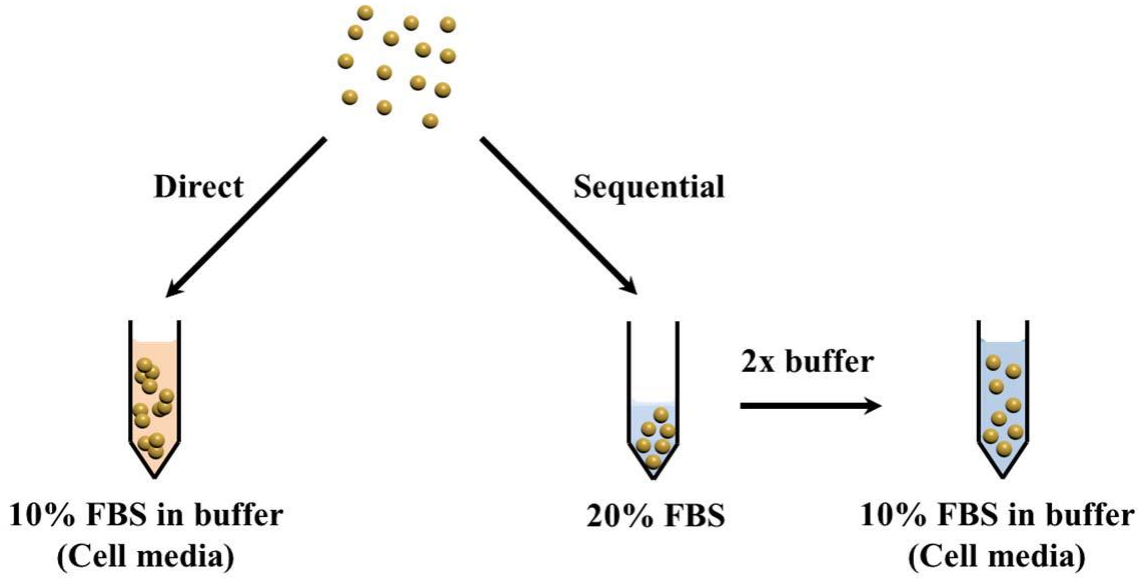

Scheme 3.2. Setting up μ-Slide for chemotaxis assay[32]. Adapted from ref 32. Copyright 2013 Ibidi GmbH

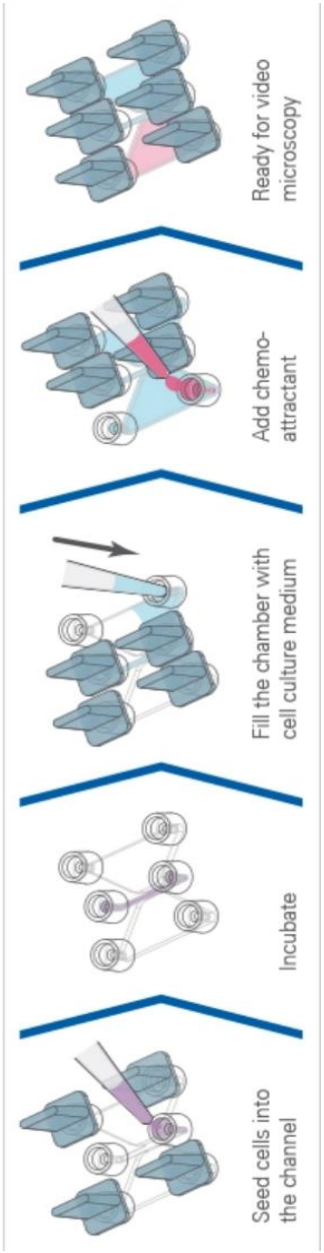

(a)

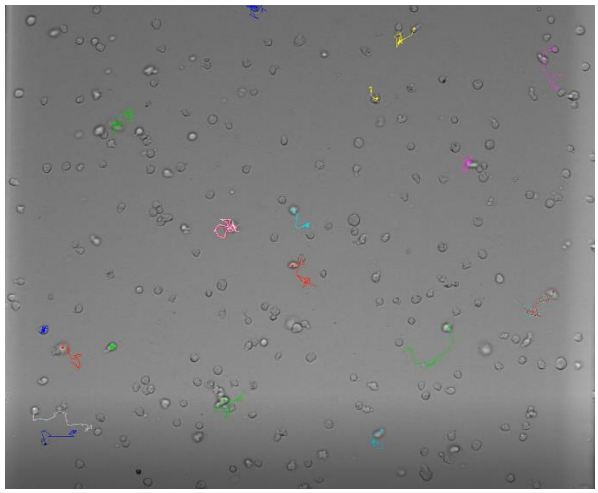

(b)

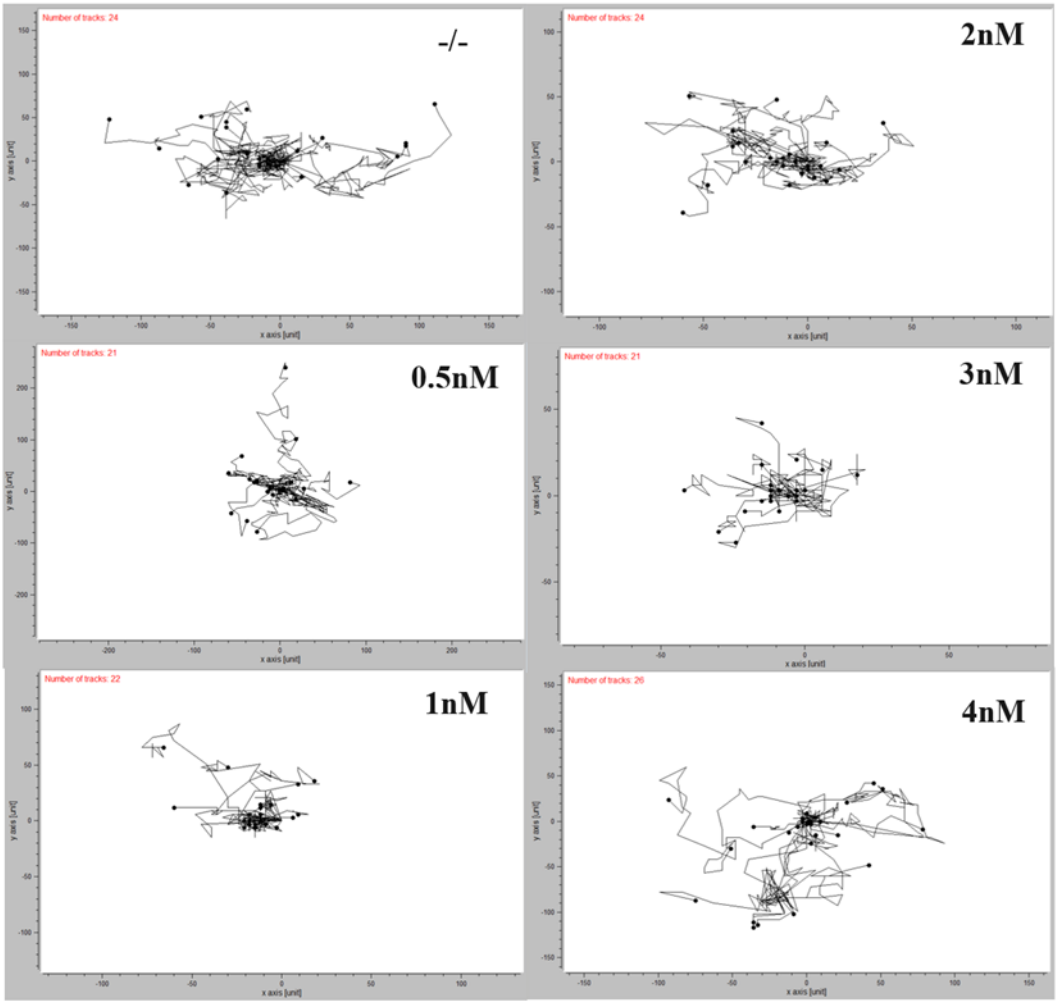

Figure 3.4. (a) The cell image for negative control and each line represents a path for one cell. (b) 2D trajectory plots for six different chemoattractant concentrations.

Negative control was also performed and labeled as (-/-). Migration along the x-axis was expected since that was the direction of the gradient. However, no obvious movement was observed.

Cell migrations were further analyzed. There were four parameters were used to evaluate the chemotactic effect at different concentrations:

The Center of mass represents the average of all single-cell endpoints, and with chemoattractant, the center of mass will be observed to move towards the source of chemoattractant.

Directness (D) is the ratio of displacement and the total path length, which indicates the efficiency of the movement. In this case, a higher D is desired with chemoattractants.

Forward migration index (FMI) is calculated by taking the ratio of displacement along one axis over the accumulated distance. It represents the efficiency of the cell movement with respect to each axis. FMI_x is defined as the FMI along the gradient, and higher FMI_x is expected for chemotaxis. However, FMI_y is expected to be zero since there is no chemoattractant gradient along the y direction.

Rayleigh test (p-value) is a statistical test for uniformity of the radial distribution of endpoints. A higher p-value indicates a more homogenous distribution around the origin. With the presence of chemoattractant, a low p-value (<0.05) is expected.

All the parameters of six different concentrations were summarized in Table 3.2. Both directness and the movement of the center of mass were very minimum for all six sets of experiments. Two FMI values were negligible. The p-value for Rayleigh tests fluctuated greatly and along with other parameters, they all lead to the conclusion that these six concentrations did not induce enough movement for further experiments. The Rayleigh test is very sensitive to outlier and adding or removing one point can lead to great fluctuations.

Table 3.2. More concentrations (0.3nM, 3nM, 10nM, 20nM, 4μM and 50ng/mL) were tested to cover a wider range (Table 3.3.). Important parameters of chemotaxis assay with six different concentrations. No ideal concentration was found for further experiments.

	Center of mass	**Directness**	**FMI_x**	**FMI_y**	**Rayleigh test**
-/-	(-7.85, 13.9)	0.214	-0.049	0.052	0.032
0.5 nM	(-10.2, 18.7)	0.188	-0.044	0.07	0.0428
1 nM	(-14.7, 10.5)	0.210	-0.142	0.052	7.85×10^{-5}
2 nM	(-19.8, 4.03)	0.161	-0.082	0.011	0.022
3 nM	(-4.5, 21.7)	0.266	-0.011	0.088	0.132
4 nM	(-10.6, 10.5)	0.262	-0.181	0.034	5.44×10^{-5}

Table 3.3. Important parameters of chemotaxis assay with a wider range of concentration. No ideal concentration was found for further experiments.

	Center of mass	**Directness**	**FMI_x**	**FMI_y**	**Rayleigh test**
3 nM	(13.1, -7.62)	0.151	0.028	-0.012	0.217
4 µM	(8.87, 18.7)	0.21	-0.010	-0.031	0.0428
50 ng/mL	(-4.2, 16.35)	0.184	-0.050	-0.122	1.25×10^{-5}
10 nM	(-11.3, -6.63)	0.115	0.012	-0.011	0.127
20 nM	(-5.1, -14.4)	0.266	0.048	-0.034	0.144
30 nM	(-10.2, 18.7)	0.188	-0.044	0.070	0.043

No noticeable migration was observed and the analytical analysis was consistent with the observation.

3.4.4. Determination of N-formyl peptide concentration

With the fluorescein tag, the concentration of N-formyl peptide in each working aliquot can be determined with UV-vis spectroscopy. Fluorescein standards were made and UV-vis spectra were collected (Figure 3.5a). The calibration curve (Figure 3.5b) was made from the Absorbance at λ=235 nm. The experimental concentration of each N-formyl peptide was 53 μM while the theoretical concentration calculated based on the information from the peptide container was 40 μM.

3.4.5 Evaluate the chemotactic effect of HDF and PDGF

The stability of three types of gold nanoparticles (citrate, PSS, PDADMAC) was tested in DMEM-BSA media. Zeta potential of DMEM-BSA was first measured and gave a value of -12.5 mV. With a negative zeta potential, positively charged PDADMAC particles were expected to be more likely to aggregate. 0.004 nM Au NP water solution was mixed with an equal volume of DMEM-BSA media to get a 0.002 nM Au NP solution in media, and this concentration is double the concentration of the desired for the experiments. No obvious aggregation was observed after the mixing of Au NPs and with media. The mixtures were incubated in the incubator (37 ºC, 5% CO_2) overnight, still no obvious aggregation was observed.

The ibidi μ-Slide Chemotaxis was used to observe the chemotactic effect and the experiment workflow was conducted as mention in section 3.3.3. 12 ng/mL was chosen as the concentration to start with as the literature value[38]. Six different concentrations (0 ng/mL, 5 ng/mL, 10 ng/mL, 12ng/mL, 15 ng/mL and 20 ng/mL) were tested for the most suitable concentration for

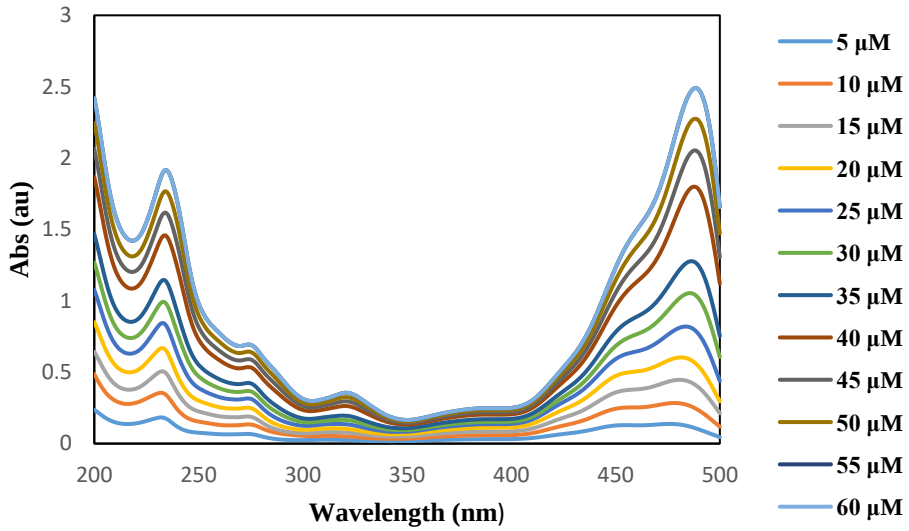

(a)

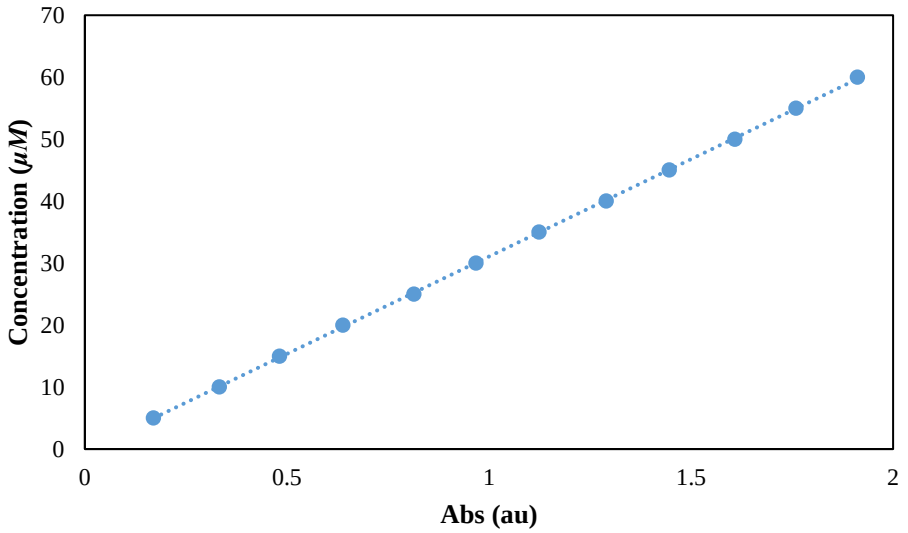

(b)

Figure 3. 5. (a) UV-vis spectra for fluorescein standards and the absorbance at λ=523 nm was recorded. (b) Calibration curve for fluorescein (y = 31.42x - 0.3528) with R^2 = 0.9999.

further studies. 2D trajectory plots are displayed in Figure 3.5 and statistical analysis results are summarized in Table 3.4. Both 2D trajectory plots and statistical analysis agreed with each other, yet none of these concentrations has significant migration to conclude chemotaxis happened.

3.5 Conclusion

The N-formyl peptide does not have a chemotactic effect on THP-1. A wide range of concentrations was tested yet no significant chemotactic migration was observed. The phenomenon was only reported by one paper and this result can be non-reproducible.

The concentration for HDF cells to respond to PDGF was not identified. The effective concentration for the collagen matrix gel has not been reported in previous studies so the 12ng/mL literature value might not apply to this study. Concentration tested only covered within two-folds of the literature value, which don't seem wide enough.

3.6 Future directions

One direction to proceed with the THP-1 project is to replace N-formyl-Nle-Leu-Phe-Nle-Tyr-Lys with fMLF, which is a more broadly used chemoattractant for monocytes.

More concentrations of PDGF need to be tested. Another concern is that the speed of HDF's movement was significantly slower than the THP-1 cell, which makes changing the collagen percentage (1.5%) in the gel a possible direction. The higher the percentage of collagen leads to larger resistance for the cell to travel. As an adherent cell line, HDF experienced more resistance. Lowering the collagen concentration can make the chemotaxis response more significant since cells are more likely to move freely. The time interval between each image is taken can be adjusted according to how fast cells travel within the gel.

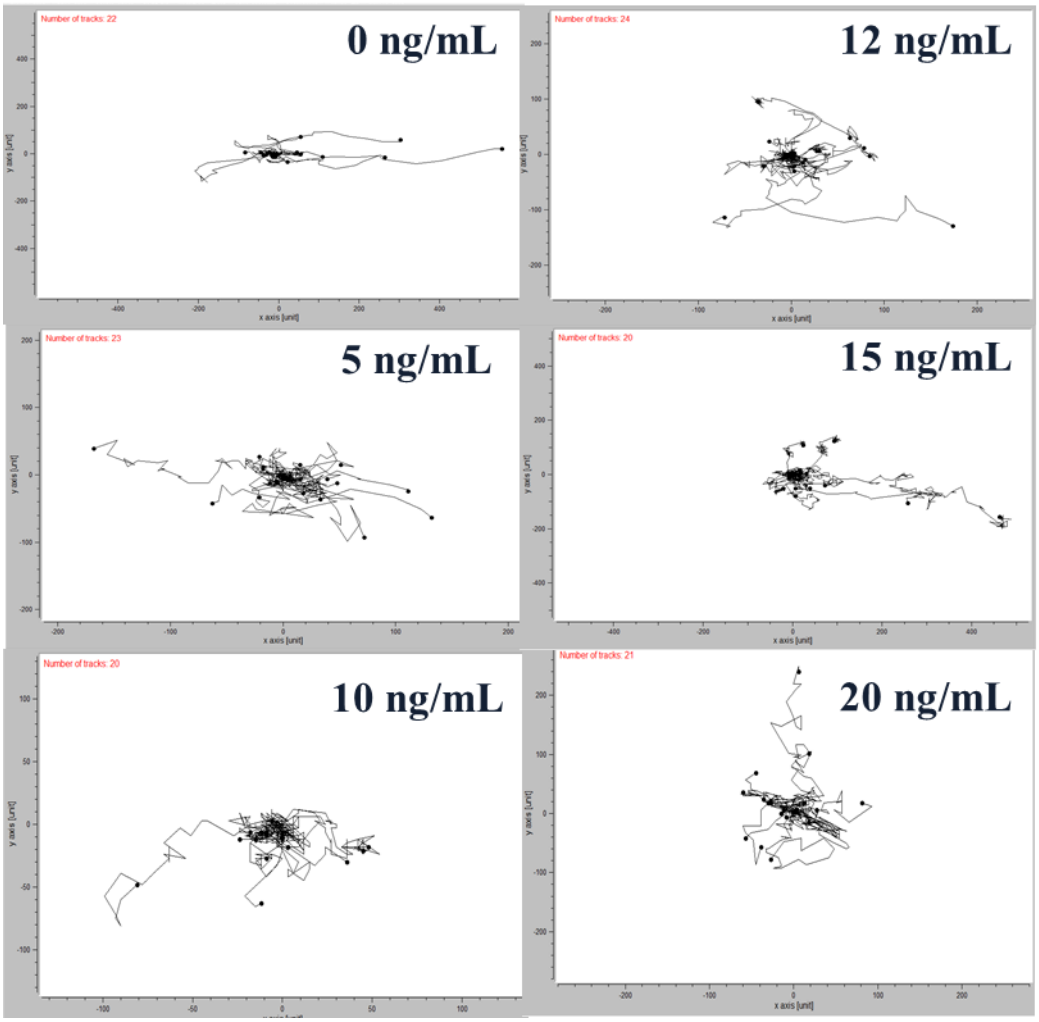

Figure 3.6. 2D trajectory plots for HDF in the presence of various concentrations of PDGF. Cell movements did not look directional.

Table 3.4. Analytical analysis of PDGF's chemotactic effect on HDF. None of the concentration points to the conclusion that cell moved directionally at any of these concentrations.

	FMI_x	**FMI_y**	**Rayleigh test**
0 ng/mL	0.103	0.092	1.0×10^{-4}
5 ng/mL	-0.041	0.037	0.011
10 ng/mL	-8.3×10^{-5}	-6.1×10^{-3}	0.546
12 ng/mL	-0.047	0.040	2.9×10^{-3}
15 ng/mL	0.012	-0.015	0.144
20 ng/mL	-0.045	0.033	0.72

After the effective concentrations are identified, viability tests need to be conducted in the presence of Au NPs. Cells will be incubated with Au NPs (0.001nM) overnight at 37^{o}C, 5% CO_2.

Then the interventions of Au NPs can be explored starting with five basic experiment sets: negative control (media: media), positive control (chemoattractant: chemoattractant), chemoattractant along, Au NPs along and lastly the combination of chemoattractant and Au NPs. A decrease of cell movement is expected due to the interaction between chemoattractant with Au NPs.

3.7 Reference

1. Colvin, V. L. The potential environmental impact of engineered nanomaterials.*Nature Biotechnol*. **2003**, 21, 1186-1170.
2. Nel, A.; Xia, T.; Madler, L.; Li, N. Toxic potential of materials at the nanolevel. *Science*. **2006**, 311, 622-627.
3. Klaine, S. J. et al.Nanomaterials in the environment: behavior, fate, bioavailability, and effects. *Environ. Toxicol. Chem.* **2008**, 27, 1825-1851.
4. Nel, A. E. et al. Understanding biophysicochemical interacions at the nano-bio interface. **Nature Mater**. *2009*, 8, 543-557.
5. Fairbrother, A.; Fairbrother, J. R. Are environmental regulations keeping up with innovation? A case study of the nanotechnology industry. *Ecotoxicol. Environ. Safety*. **2009**, 2, 1327-1330.
6. Dix, D. J.et al. The ToxCast program for prioritizing toxicity testing of environmental chemicals. *Toxicol. Sci*. **2007**, 95, 5-12.
7. Murphy, C. J.; Vartanian, A. M.; Geiger, F. M.; Hamers, R. J.; Pedersen, J.; Cui, Q.; Haynes, C. L.; Carlson, E. E.; Hernandez, R.; Klaper, R. D.; Orr, G. Biological responses to engineered nanomaterials: needs for the next decade. *ACS Central Science*. **2015**, 1, 117-123. PMID 27162961.
8. Keller, A. A.; Lazareva, A. Predicted releases of engineered nanomaterials: from global to regional to local. *Environ. Sci. Technol. Lett*. **2014**, 1, 65-70.
9. Sykes, E. A. et al. Tailoring nanoparticle designs to target cancer based on tumor pathophysiology. *Proc. Natl. Acad. Sci. USA* **2016**, 113, E1142-E1151.
10. Sisco, P. N.; Minrova, E.; Wilson, C.; Murphy, C. J.; Goldsmith, E. C. The effect of gold nanorods on cell-mediated collagen remodeling. *Nano Lett.* **2008**, 8, 3409-3412. PMID: 19077195.
11. Sisco, P.N; Murphy, C. J. et al. Adsorption of cellular proteins to polyelectrolytefunctionalized gold nanorods: a mechanism for nanoparticle regulation of cell phenotype?" *PLoS ONE*. **2014**, 9(2): e86670.
12. Yang, J. A.; Phan, H. T.; Vaidya, S.; Murphy, C. J. Nanovacuums: nanoparticle uptake and differential cellular migration on a carpet of nanoparticles. *Nano Lett*. **2013**, 13, 2295-2302. PMID 23577660.
13. Grzincic, E. M.; Yang, J. A.; Drnevitch, J.; Lotsch, P. F.; Murphy, C. J. Global transcriptometic analysis of model human cell lines exposed to surface-modified gold nanoparticles: the effect of surface chemistry. *Nanoscale* **2015**, 7, 1349-1362.
14. Grzincic, E. M.; Murphy, C. J. Gold nanorods indirectly promote migration of metastatic human breast cancer cells in three-dimensional cultures. *ACS Nano* **2015**, 9, 6801-6816. PMID 26118624.
15. Falagan-Lotsch, P.; Grzincic, E. M.; Murphy, C. J. One low-dose exposure of gold nanoparticles induces long-term changes in human cells. *Proc. Natl. Acad. Sci. USA* **2016**, 113, 13318-13323. PMID 27821760.
16. Chisholm, Hugh, Chemotaxis . *Encyclopædia Britannica*. **1911**. Cambridge University Press. p. 77.
17. de Oliveira S; Rosowski .E.E; Huttenlocher A. Neutrophil migration in infection and wound repair: going forward in reverse. *Nature Reviews. Immunology*. **2016**.16 (6): 378–91. PMC 5367630. PMID 27231052.

18. Stuelten C.H.; Parent C.A. Montell DJ Cell motility in cancer invasion and metastasis: insights from simple model organisms. *Nature Reviews. Cancer*. **2016**. 18 (5): 296–312. PMC 6790333. PMID 29546880.
19. Patel. S.; Jung, D.; Yin, P. T.; Carlton, P.; Yamamoto, M.; Bando, T.; Sugiyama, H.; Lee, K-B. NanoScript: a nanoparticle-based artificial transcription factor for effective gene regulation. *ACS Nano* **2014**, 8, 8959-8967.
20. Zhu, M.; Nie, G.; Meng, H.; Xia, T.; Nel, A.; Zhao, Y. Physicochemical properties determine nanomaterial cellular uptake, transport, and fate. *Acc. Chem. Res*. **2014**, 46, 622-631.
21. Liu, Y.; Yang, M.; Zhang, J.; Zhi, X.; Li, C.; Zhang, C.; Pan, F.; Wang, K.; Yang, Y.; de la Fuentea, J. M.; Cui, D. Human induced pluripotent stem cells for tumor targeted therapy delivery of gold nanorods and enhanced photothermal therapy. *ACS Nano* **2016**, 10, 2375-2385.
22. Lynch, I.; Cedrvall, T.; Lundqvist, M.; Cabaleiro-Lago, C.; Linse, S.; Dawson, K. A. The nanoparticle-protein complex as a biological entity; a complex fluids and surface science challenge for the 21st century. *Adv. Colloid Interfac. Sci*. **2007**, 134-135, 167-174.
23. Cedervall, T.; Lynch, I.; Lindman, S.; Berggard, T.; Thulin, E.; Nilsson, H.; Dawson, K. A.; Linse, S. Understanding the nanoparticle-protein corona using methods to quantify exchange rates and affinities of proteins for nanoparticles. *Proc. Natl. Acad. Sci. USA* **2007**, 104, 2050-2055.
24. Cedervall, T.; Lynch, I.; Foy, M.; Berggard, T.; Donnelly, C. S.; Cagney, G.; Linse, S.; Dawson, K. A. Detailed identification of plasma proteins adsorbed on copolymer nanoparticles. *Angew. Chem. Int. Ed*. **2007**, 46, 5754-5756.
25. Lundqvist, M.; Stigler, J.; Elia, G.; Lynch, I.; Cedervall, T.; Dawson, K. A. Nanoparticle size and surface properties determine the protein corona with possible implications for biological impacts. *Proc. Natl. Acad. Sci. USA* **2008**, 105, 14265-14270.
26. Zhao, X.; Jain, S.; Larman, H. B.; Gonzalez, S.; Irvine, D. J. Directed cell migration via chemoattractants released from degradable microspheres. *Biomaterials* **2005**, 26, 5048-5063.
27. Sozzani, S; Zhou, D; Locati, M; Bernasconi, S; Luini, W; Mantovani, A; O'Flaherty, J. T. Stimulating properties of 5-oxo-eicosanoids for human monocytes: Synergism with monocyte chemotactic protein-1 and -3. *Journal of Immunology*. **1996**. 157 (10): 4664–71. PMID 8906847.
28. Hannink M, Donoghue DJ. Structure and function of platelet-derived growth factor (PDGF) and related proteins. *Biochim. Biophys. Acta*. **1989**. 989 (1): 1–10. PMID 2546599.
29. Heldin, C.H. Structural and functional studies on platelet-derived growth factor. *EMBO J*. **1992**. 11 (12): 4251–4259. PMID 1425569.
30. Perrault, S. D.; Chan, W. C. W. Synthesis and Surface Modification of Highly Monodispersed, Spherical Gold Nanoparticles of 50-200 nm. *J. Am. Chem. Soc*. **2009**, 131, 17042–17043.
31. Ibidi GmbH. *Application 17*. **2014**, Version 2.4.
32. Ibidi GmbH. *Application 24*. **2014**, Version 2.4.
33. Yang, J. Studies at the nanoparticle-biomolecular interface and beyond. Thesis， **2013**， University of Illinois at Urbana Champaign.
34. Prossnitz, Eric R., and D. Ye Richard. The N-formyl peptide receptor: a model for the study of chemoattractant receptor structure and function. *Pharmacology & therapeutics* **1997**, 73-102.

35. Czapiga, Meggan, Ji-Liang Gao, Allan Kirk, and Julie Lekstrom-Himes. Human platelets exhibit chemotaxis using functional N-formyl peptide receptors. *Experimental hematology* , **2005**, 73-84.
36. Fletcher, Mark P., and John I. Gallin. Human neutrophils contain an intracellular pool of putative receptors for the chemoattractant N-formyl-methionyl-leucyl-phenylalanine. **1983**, 792-799.
37. Gao, Ji-Liang, and Philip M. Murphy. Species and subtype variants of the N-formyl peptide chemotactic receptor reveal multiple important functional domains. *Journal of Biological Chemistry*, **1993**, 25395-25401.
38. Li, Wei, Jianhua Fan, Mei Chen, Shengxi Guan, David Sawcer, Gary M. Bokoch, and David T. Woodley. Mechanism of human dermal fibroblast migration driven by type I collagen and platelet-derived growth factor-BB. *Molecular biology of the cell*. **2004**. 94-309.